

Article

Seawater Intrusion on the Arctic Coast (Svalbard): The Concept of Onshore-Permafrost Wedge

Marek Kasprzak 

Institute of Geography and Regional Development, University of Wrocław, plac Uniwersytecki 1, 50-137 Wrocław, Poland; marek.kasprzak@uwr.edu.pl

Received: 7 July 2020; Accepted: 1 September 2020; Published: 3 September 2020



Abstract: Numerous hydrogeological studies on the coastal zone describe the intrusion of sea water inland, salting underground aquifers. The phenomenon is commonly observed in the coasts outside polar areas. However, the impact of sea water has so far not been an object of detailed investigation in a periglacial environment devoid of subsea permafrost. Geophysical measurements at the west coast of the Wedel-Jarlsberg Land in Svalbard indicate that the border between the unfrozen seabed and the frozen ground onshore is not delimited by the shoreline. A zone of coastal unfrozen ground is located under a thin layer of permafrost reaching toward the sea. This state was observed with the use of electrical resistivity tomography under rocky headlands and capes, uplifted marine terraces located at the foot of mountain massifs and valley mouths as well as in the marginal zone of the Werenskiöld Glacier. This short article presents the results of such a measurement, supplemented with electromagnetic detection. The measurements are unique in that they were conducted not only on the land surface, but also at the floor of the sea bay during the low water spring tide. The author proposes name structures detected in the coastal zone as a “permafrost wedge”, extending an identification of the permafrost base between the coast and the glaciers of Svalbard. However, in the absence of boreholes that would allow determining the thermal state of the ground in the study sites, the concept is based only on the interpretation of the geophysical imaging. Therefore, further discussion is required on whether the identified contrasts in electrical resistivity indeed result from thermal differences between the rocks or if they only indicate the cryotic state of the ground (saline cryopeg) within the range of seawater intrusion.

Keywords: permafrost base; permafrost wedge; seawater intrusion; coast; electrical resistivity tomography; electromagnetic induction; geophysical imaging; Spitsbergen; Svalbard; Arctic

1. Introduction

Hydrogeological investigations performed in a number of locations worldwide confirm the strong impact of the sea water percolating deep in the ground toward inland due to the difference in density between salt and fresh groundwater [1–10]. In the coastal zone, sea water forms an intrusion propagating under the non-saline rock layers just below the ground surface. This type of contact zone has been described among others on carbonate islands and coasts [11,12]. Saline water is found in boreholes and may be well recognized with the use of geophysical methods [12–20].

These brief descriptions allow for an assumption that the impact of saline water should be analogical along the coast in the periglacial zone, where permafrost is developed onshore. An example can be found on the west coast of Spitsbergen, the largest island in the Svalbard archipelago. Despite a good understanding of the characteristics of the local permafrost obtained from numerous boreholes and measurement points [21,22], the question of its evolution in the contact zone with the sea remains open. The problem has not been solved by hydrogeological observations either, and examinations of water flows under the permafrost have not focused directly on the coastline [23–25]. However,

the possibility of saline water intrusions and heat wave from the sea was indicated by the geophysical measurements performed by the author in the years 2012–2017 in Wedel-Jarsberg Land between Skoddebukta (bay) in the north and Hornsund (fjord) in the south [26–28]. The sea water impact was detected in the grounds of each of the investigated coastline sections with various lithologies (schists, quartzites, marbles) and morphologies (under rocky headlands and capes, uplifted marine terraces at the feet of mountain massifs and valley mouths as well as in the marginal zone of the Werenskiold Glacier, see sites 1–3 in Figure 1). This has also been confirmed in recent research conducted in Svalbard by other authors, who observed water flow within the permafrost [29] and thawing of deeper ground layers in contact with saline water [30]. Similarly, changes in the geophysical properties of deeper ground are known from the coast of West and North Greenland [31] or the Canadian territory of Nunavut [32].

This article aims at both proposing a model of seawater impact on the coasts of the High Arctic and initiating a discussion. The model applies to regions with no subsea permafrost presence or where it lies deeper under the seabed, which would limit the percolation of saline water into the ground [33–35]. Although the assumptions for the model have already been developed [26] and are based on the above-mentioned research, this article presents the results of an additional, representative geophysical imaging. It is unique in that it jointly shows the cross-section of the part under the floor of a marine embayment and the adjacent onshore part. The measurement was possible when the sea floor was exposed during the low water spring tide in Nottinghambukta (Figure 1). Finally, it is possible to show the shape of the permafrost from the shoreline to the fronts of glaciers filling the Svalbard valleys, completing the known schemes [36,37].

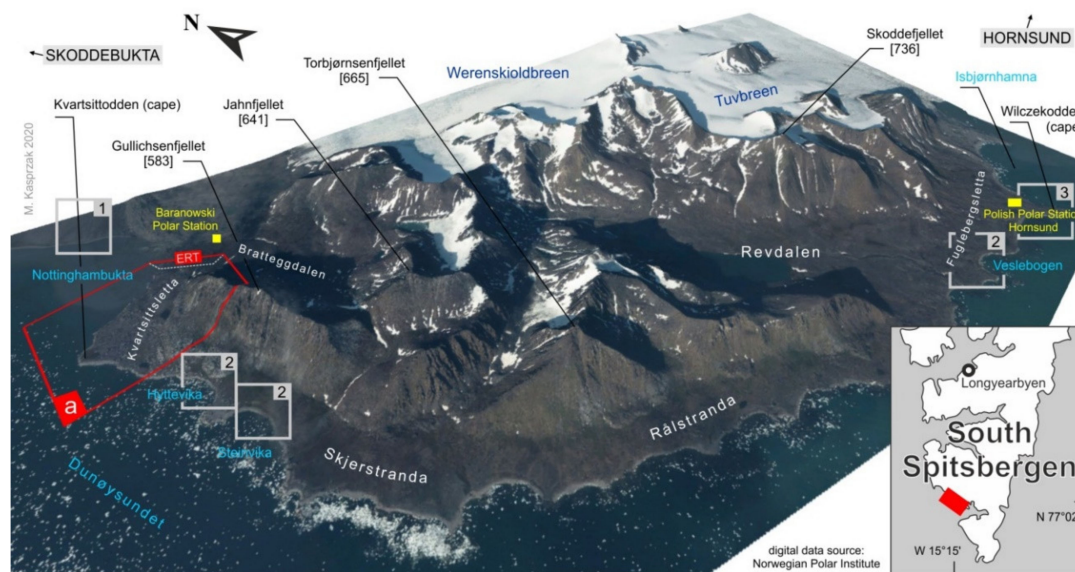


Figure 1. The west coast of Spitsbergen between Skoddebukta (bay) in the north and Hornsund (fjord) in the south: **a**—study area shown in Figures 2 and 3, ERT—electrical resistivity tomography section presented in this study, **1**—location of near-surface geophysical imaging of schist bedrock published in [28], **2**—location of near surface geophysical imaging of quartzite and marble bedrock published in [26], **3**—location of near surface geophysical imaging of marble and schists bedrock published in [27]. The figure is based on Norwegian Polar Institute digital data.

The study area is a typical example of a rocky coast in Svalbard, free of glacier ice and subjected to the influence of relatively warm sea water. The investigated bedrock is formed of mica schists and quartzites [38]. The coastline is in the form of a rock cliff, with uplifted marine terraces of Kvarfittsletta above. In the north, the cliff ends at the mouth of the Brattegg Valley, in the vicinity of the Stanisław Baranowski Polar Station. Near-surface parts of the ground are thermally monitored in that area [39].

The measurements revealed a deep (1.5–4 m) permafrost active layer, with the maximum thawing reached in mid-August.

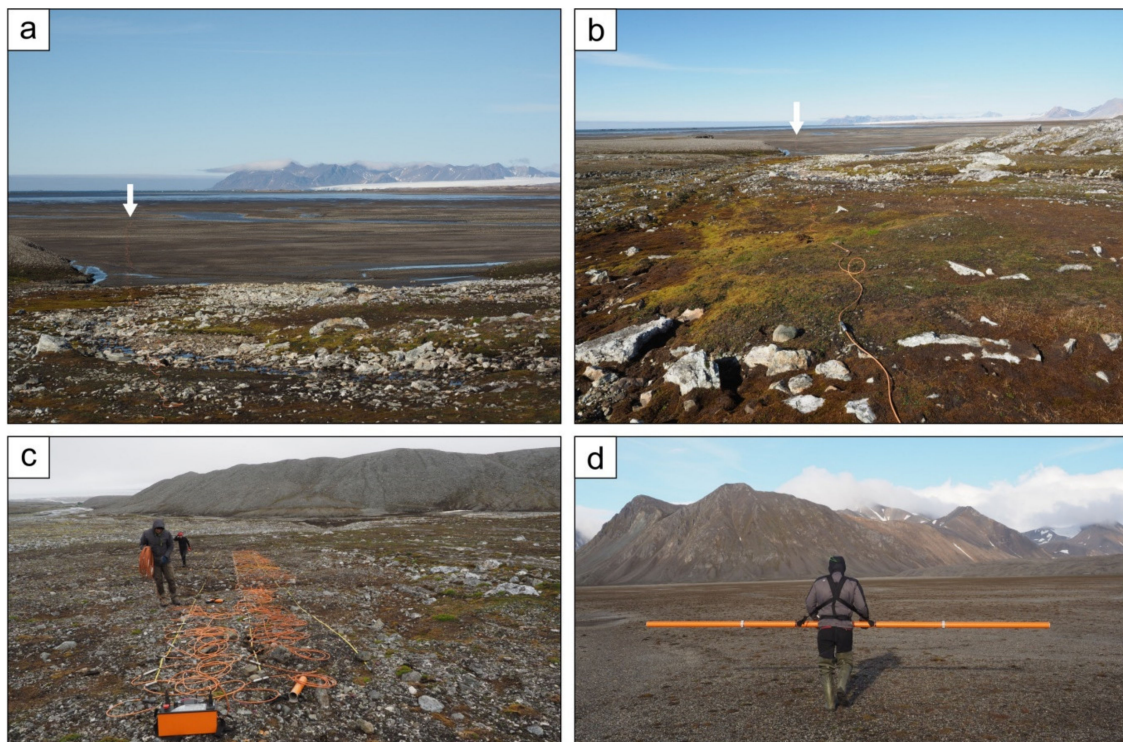


Figure 2. Illustrative photos documenting the study area and research methods: (a) the exposed bottom of Nottinghambukta (bay) during low water spring tide, the arrow marks the beginning of the ERT section, (b) the same ERT section from the hinterland, (c,d) ERT and EMI devices (during measurements at other sites). Photographed by M. Kasprzak.

2. Methods

The properties of the bedrock in the coastal zone were identified with the use of electrical resistivity tomography (ERT). This method is commonly used to detect the presence of permafrost and various types of ground ice (e.g., [40–47]). ERT, which is basically a combination of electrical resistivity sounding and profiling, consists of the measurements of resistivity (R) in a number of four-electrode arrays, in which electric current (I) is transmitted to earth by two electrodes (C_1, C_2), and voltage–potential difference (V) is measured by the second pair of electrodes (P_1, P_2). As the rock medium is not a uniform body, the measured resistivity, expressed as the ratio between voltage and current with allowance for coefficient (k), which depends on the electrode array and the distances between the electrodes, is apparent resistivity (ρ_{app}). Good vertical resolution and depth penetration were simultaneously obtained with the use of the Wenner–Schlumberger electrode array [48–50]. The device used was ARES (GF Instruments, Brno, Czech Republic) with a set of 88 electrodes. The results of the ground resistivity measurements (expressed in $\Omega\cdot\text{m}$) were subjected to standard geophysical interpretation (inversion) in RES2DINV software (Geotomo, Malaysia). The procedure was based on default smoothness-constrained inversion formulation [51].

The measurement was performed on 31 July 2017 during the low water spring tide when the sea water exposed the floor of a tidal flat in Nottinghambukta (Figure 2). The measurement section was 995 m in length, obtained using the roll-along technique including the sea floor (the first 200 m) and continued on the surface of the uplifted marine terraces toward the mouth of the Bratteg Valley, perpendicular to the shoreline. The total number of obtained data points was 5931 and the inversion model had 16 layers and 2757 blocks.

Due to the 5 m spaces between the electrodes, the inversion model could not include the superficial layer, which was therefore additionally examined with the use of electromagnetic induction (EMI) [52,53]. This method allowed one to obtain images of the permafrost active layer [54]. The measurements were carried out with an electromagnetic conductivity meter CMD-Explorer (GF Instruments, Brno). The device is a portable tube that contains both transmitter and receiver coils inside at dipole center distances of 1.48, 2.82, and 4.49 m, which allow for measurements of apparent electrical conductivity/resistivity with the maximum sampling rate of 10 Hz (the effective depth ranges were at 1.1, 2.2, and 3.4 m simultaneously). The measurement results were presented graphically with the use of digital data from the Norwegian Polar Institute, processed in Metashape v 1.6.3. (Agisoft), Global Mapper v16.0.1. (Blue Marble), and ArcScene v10.8 (ESRI) software.

The analysis of the measurement results was based on the fact that rocks cooled to temperatures below 0 °C drastically reduce their ability to conduct electric current [50]. The published interpretations (e.g., [42,43,54,55]) support an assumption that resistivity approximating or exceeding 1 k $\Omega\cdot$ m may indicate frozen ground (Figure 3), although the literature gives very different threshold values depending on local ground features including groundwater salinity.

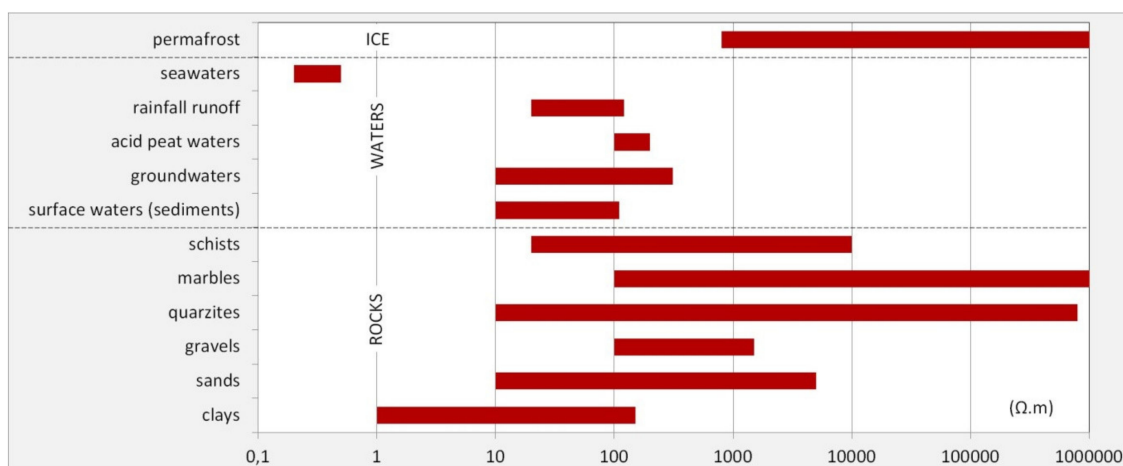


Figure 3. Range of resistivity for different materials. Compilation based on [44,49,50,56,57].

3. Results

The inversion model resulting from the ERT measurements indicates highly contrasting ground resistivity (Figure 4a). The similarity to the results obtained in the geoelectric measurements cited above allowed for a tentative assumption that this contrast was due to the negative temperatures of the rocks and ground ice presence onshore. The ground under the floor of Nottinghambukta showed low resistivity values (ρ from 1 to 500 $\Omega\cdot$ m), which practically eliminates the possibility of ground ice presence in this zone. The rocks under the terrestrial part showed extremely high resistivity values ($\rho > 10,000 \Omega\cdot$ m), which are characteristic of permafrost. These values indicate practically no electric conductivity and mask all local lithological differences. In this zone, the near-surface ground layer also showed lower resistivity values, which were related to the permafrost active layer and penetration of fresh groundwater. This phenomenon is particularly well visible at about 820–890 m of the ERT section. The area is located at the foot of a mountain slope, which supplies meltwater. Here, the ground thawing in summer, identified with the use of the above method, can be assumed to reach at least 10–20 m under the surface.

has the shape of a near-vertical wall (resembling a cliff line), although the analysis of the apparent resistivity suggests that it may just have the shape of a cavity retreated toward the land.

4. Discussion

The combined results of the ERT and EMI measurements allowed for better geophysical imaging of the coastal bedrock than the previous geophysical measurements in the Wedel-Jarlsberg Land [26–28]. Extending the measurement section along the exposed sea floor of the bay proved to be of key importance. As was the case in the previous geophysical images, the ERT inversion model demonstrated high electrical resistivity contrast of the ground between the land and the sea. Low resistivity obtained for the latter area, typically not exceeding $100 \Omega \cdot \text{m}$, suggests that the investigated parts of the seabed are not frozen. The extremely high values, which continue regardless of the varying lithology, indicate the presence of permafrost, although the literature review clearly refutes the possibility of finding a limit value for the presence of permafrost with spatially varying environmental factors. There are also examples of resistivity much lower than $1 \text{ k}\Omega \cdot \text{m}$ found for permafrost (e.g., [47]).

This article indicates that the border between high and low electrical resistivity values of rocks in the coastal zone has a specific shape. At greater depths, the low-resistivity body penetrates inland from the sea side and shows as seawater intrusion (Figure 5). The high-resistivity body at the surface forms a wedge, which is attached to the land side and diminishes in thickness toward the sea. Unlike saline intrusions observed at lower latitude coasts, the landward impact of sea water is limited by the presence of permafrost. An assumption can thus be made that in the west coast of Svalbard, and probably also in other sections of polar coasts subjected to neotectonic uplift and lacking subsea permafrost, or where subsea permafrost is found at greater depths below the seabed [58,59], the near-sea terrestrial part of permafrost assumes a characteristic shape that will be referred to here as a “permafrost wedge”. Below it, the contact between rocks having different thermal properties most likely assumes the shape of a cavity. The described observation resembles ground-temperature distribution and a tongue of developing permafrost in front of the retreating glacier [36,37]. Such an analogy makes it possible to draw a simple diagram suitable for the coasts of Svalbard, in which the permafrost, bounded on one side by the glacier and on the other side by the sea, take a similar shape (Figure 6). More complicated is the form of the interface between the frozen and unfrozen ground. This must be set by the diffusion of heat landward from the sea-covered ground and have an impact on the properties of permafrost far inland, which can be indirectly seen in the ERT measured apparent resistivity pseudosection (Figure 4).

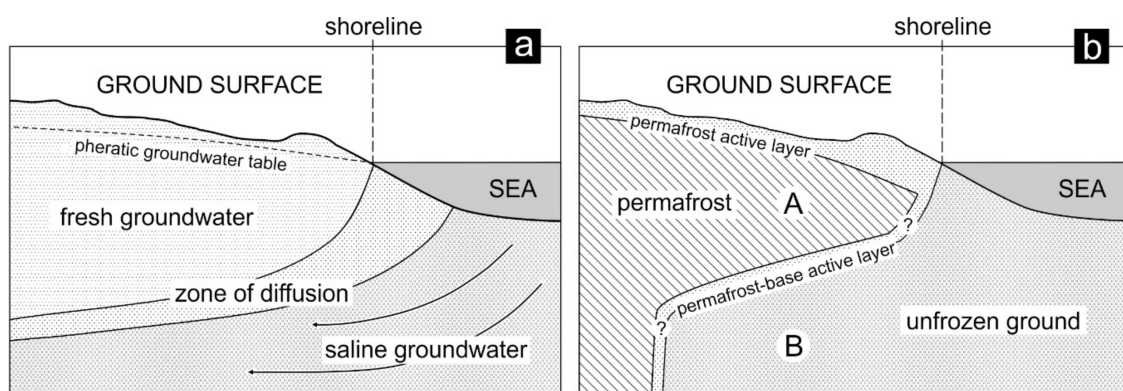


Figure 5. The onshore impact of sea water: (a) salt water intrusion in a coastal aquifer; (b) permafrost range limited by seawater, based on [1], A—“permafrost wedge”, B—seawater intrusion/heat wave effect.

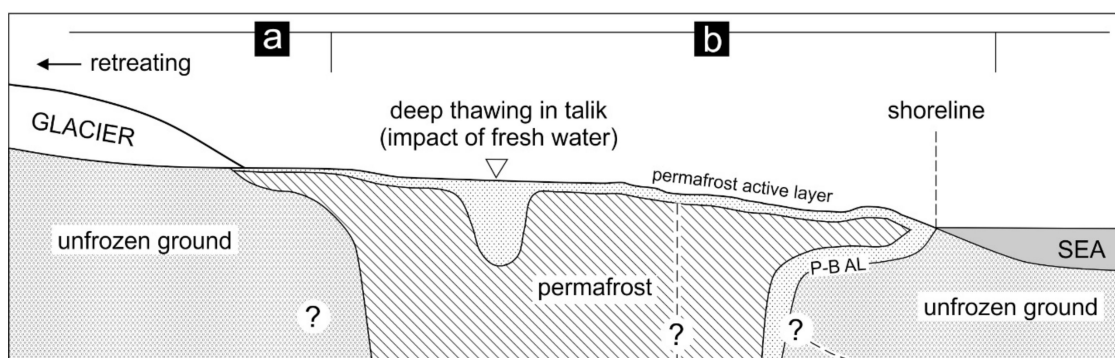


Figure 6. A conceptual model of the permafrost between the sea coast and the glacier front: (a) based on glaciological research [36,37], (b) based on geophysical imaging; P-B AL—permafrost-base active layer (?); vertical dashed line drawn in permafrost to distinguish ground with different apparent resistivity (reference to the ERT measured apparent resistivity pseudosection in Figure 4).

The presented interpretation is tentative, as the results of the geoelectric measurements can only be treated as indirect evidence of rock temperatures. At this stage of research, prior to thermal measurements in boreholes penetrating through the “permafrost wedge”, the possibility still exists that the seawater intrusion only causes a change in the salinity of waters in the rock medium of the land part of the coast. With higher salinity, the ground can be unfrozen even at temperatures of -2 to -3 °C [60,61]. Measurements of temperature and chemical/structural properties of saline soils [62] demonstrated a shift of the phase transition of groundwater on average from -0.4 to -1.6 °C (frozen) and from -0.6 to -3.5 °C (thawed) for soils having a low degree of salinity as well as -1.2 to -21.8 °C (frozen) and -4.9 to -41.0 °C (thawed) at a high degree of salinity. In the bays of the Greenland Sea, in the Hornsund zone, at depths greater than 50 m, seawater salinity is in the range of 34.7–34.9 PSU (practical salinity unit, based on the properties of seawater conductivity, $\text{PSU} \cong \text{salinity } \text{‰}$) [63,64]. At the bottom of Skoddebukta (bay), which neighbors the study area, the measured salinity was 33.5–34.5 PSU [65,66]. For comparison, the mineralization of water flowing from the springs located in front of the Werenskiöld Glacier typically does not exceed $75 \text{ mg}\cdot\text{L}^{-1}$ and may exceed $200 \text{ mg}\cdot\text{L}^{-1}$ only during periods of intensive thawing processes [67,68]. In this hypothetical situation, lower freezing point would cause the underwaters within the marine intrusion to still have a sub-zero temperature, while the ground would be in a cryotic condition as in marine cryopegs.

The interpretation presented here, however, is supported by the measurements of seawater temperature. In the near-surface zone in the winter, the water temperature decreases to approx. -2 °C, but in the summer, it warms to $+3$ to $+6$ °C [64]. An even higher seawater temperature was measured by the author with the use of a submerged HOBO temperature datalogger in Hytttevikka (bay), which is protected by skerries from the open sea. On 11 August 2017, the temperature was 7.8 °C, while the temperature of the permafrost in Svalbard, as given in older studies [69] and measured from boreholes at a depth of 30 m, was -3.0 °C and -2.4 °C at the mineralization of aquifers in the range of 34 – $44 \text{ mg}\cdot\text{L}^{-1}$. Seawater temperature variations of this scale lead to the conclusion that the bottom part of the “permafrost wedge”, together with the rest of the permafrost contact zone subjected to annual seawater temperature variations, forms a permafrost-base active layer. This would be consistent with observations of seasonal active layer associated with subsea permafrost found in sediments of nearshore shallow waters in Prudhoe Bay in the Beaufort Sea in Alaska [70].

5. Conclusions

The summary of the data presented in this article can be listed as three main points.

Unique measurements using the electrical resistivity tomography performed on the floor of the sea bay and at the same time on the land in the area of Spitsbergen west coast confirmed the results of earlier geophysical imaging in this zone and the presence of seawater intrusion reaching inland.

Seawater intrusion inland causes the formation of structures referred here to as a “permafrost wedge”. The “permafrost wedge” is the near-surface part of the land-side permafrost. It can be 60 m in length and 20 m in thickness, decreasing toward the shoreline. These values, however, depend on the morphology of the coast. The “permafrost wedge” resembles ground-temperature distribution and a tongue of developing permafrost in front of the retreating glacier.

No conclusive evidence has been found on whether the seawater intrusion causes the increase in the temperature of the deeper zones of the ground on the coast or just a phase change related to the shifting of the freezing point due to salinity. The proposal that the zone actually thaws is, however, supported by high seawater temperatures in the summer, which temporarily exceed 6–7 °C. In addition, annual seawater temperature variations suggest that the bottom part of the “permafrost wedge” and the entire contact zone below are annually subjected to changes in the thermal state, forming a permafrost-base active layer. This hypothesis will need to be verified by temperature measurements in boreholes penetrating the “permafrost wedge”.

Funding: This research was financially supported by research project No. 2015/19/D/ST10/02869 of the National Science Center, Poland.

Acknowledgments: Used aerial photographs of the Norwegian Polar Institute were purchased as part of the order ZP. 2420.1.IGRR.ZG.2013 (2013-01-9) financed from statutory funds of the Institute of Geography and Regional Development, University of Wrocław. The author thanks Michał Łopuch and Kacper Marciniak for their valuable field assistance.

Conflicts of Interest: The author declares no conflict of interest. The funders had no role in the design of the study; in the collection, analyses, or interpretation of data; in the writing of the manuscript, or in the decision to publish the results.

References

- Cooper, H.H., Jr.; Kohout, F.A.; Henry, H.R.; Glover, R.E. *Sea Water in Coastal Aquifers*; US Government Printing Office: Washington, DC, USA, 1964; pp. C1–C84.
- Oude Essink, G.H.P. *Density Dependent Groundwater Flow Salt Water Intrusion and Heat Transport. KHTP/GWM II Hydrological Transport Processes/Groundwater Modelling II*; Utrecht University: Utrecht, The Netherlands, 2002.
- López-Geta, J.A.; de Dios Gómez, J.; Orden, J.A.d.l.; Ramos, G.; Rodríguez, L. (Eds.) *Coastal Aquifers Intrusion Technology: Mediterranean Countries. The state of sea Intrusion in Coastal Aquifers of the Mediterranean and Assessment Techniques*; Publicaciones del Instituto Geológico y Minero de España: Madrid, Spain, 2003; p. 330.
- Kirch, R. Groundwater quality—Saltwater intrusions. In *Groundwater Geophysics. A tool for Hydrogeology*, 2nd ed.; Kirch, R., Ed.; Springer: Berlin/Heidelberg, Germany, 2009; pp. 475–490.
- Kuria, Z.N.; Woldai, T.; Opiyo-Akech, N. Imaging saltwater intrusion into coastal aquifers with electrical resistivity tomography at Lamu Island, south coast Kenya. *AJST Sci. Eng. Ser.* **2010**, *11*, 57–72.
- Jørgensen, F.; Scheer, W.; Thomsen, S.; Sonnenborg, T.O.; Hinsby, K.; Wiederhold, H.; Schamper, C.; Burschil, T.; Roth, B.; Kirsch, R.; et al. Transboundary geophysical mapping of geological elements and salinity distribution critical for the assessment of future sea water intrusion in response to sea level rise. *Hydrol. Earth Syst. Sci.* **2012**, *16*, 1845–1862. [[CrossRef](#)]
- Werner, A.D.; Ward, J.D.; Morgan, L.K.; Simmons, C.T.; Robinson, N.I.; Teubner, M.D. Vulnerability Indicators of Sea Water Intrusion. *Ground Water* **2012**, *50*, 48–58. [[CrossRef](#)] [[PubMed](#)]
- Asfahani, J.; Abou Zakhem, B. Geoelectrical and Hydrochemical Investigations for Characterizing the Salt Water Intrusion in the Khanasser Valley, Northern Syria. *Acta Geophys.* **2013**, *61*, 422–444. [[CrossRef](#)]
- Lofi, J.; Pezard, P.; Bouchette, F.; Raynal, O.; Sabatier, P.; Denchik, N.; Levannier, A.; Dezileau, L.; Certain, R. Integrated Onshore-Offshore Investigation of a Mediterranean Layered Coastal Aquifer. *Groundwater* **2013**, *51*, 550–561. [[CrossRef](#)]
- Raj, A.S.; Oliver, D.H.; Srinivas, Y. Forecasting groundwater vulnerability in the coastal region of southern Tamil Nadu, India—A fuzzy-based approach. *Arab. J. Geosci.* **2016**, *9*, 351. [[CrossRef](#)]
- Myroie, J.E.; Carew, J.L. Speleogenesis in coastal and oceanic settings. In *Speleogenesis. Evolution of Karst Aquifers*; Klimchouk, A.B., Ford, D.C., Palmer, A.N., Dreybrodt, W., Eds.; National Speleological Society: Huntsville, AL, USA, 2000; pp. 226–233.
- Myroie, J.E.; Carew, J.L. Karst development on carbonate islands. *Am. Assoc. Pet. Geol.* **2003**, *1*, 1–21.

13. Comte, J.-C.; Banton, O. Cross-validation of geo-electrical and hydrogeological models to evaluate seawater intrusion in coastal aquifers. *Geophys. Res. Lett.* **2007**, *34*, L10402. [[CrossRef](#)]
14. De Franco, R.; Biella, G.; Tosi, L.; Teatini, P.; Lozej, A.; Chiozzotto, B.; Giada, M.; Rizzetto, F.; Claude, C.; Mayer, A.; et al. Monitoring the saltwater intrusion by time lapse electrical resistivity tomography: The Chioggia test site (Venice Lagoon, Italy). *J. App. Geophys.* **2009**, *69*, 117–130. [[CrossRef](#)]
15. Martínez, J.; Benavente, J.; García-Aróstegui, J.L.; Hidalgo, M.C.; Reyd, J. Contribution of electrical resistivity tomography to the study of detrital aquifers affected by seawater intrusion–extrusion effects: The river Vélez delta (Vélez-Málaga, Southern Spain). *Eng. Geol.* **2009**, *108*, 161–168. [[CrossRef](#)]
16. Morrow, F.J.; Ingham, M.R.; McConchie, J.A. Monitoring of tidal influences on the saline interface using resistivity traversing and cross-borehole resistivity tomography. *J. Hydrol.* **2010**, *389*, 69–77. [[CrossRef](#)]
17. Trabelsi, F.; Mammou, A.B.; Tarhouni, J.; Piga, C.; Ranieri, G. Delineation of saltwater intrusion zones using the time domain electromagnetic method: The Nabeul-Hammamet coastal aquifer case study (NE Tunisia). *Hydrol. Process.* **2013**, *27*, 2004–2020. [[CrossRef](#)]
18. Beaujean, J.; Nguyen, F.; Kemna, A.; Antonsson, A.; Engesgaard, P. Calibration of seawater intrusion models: Inverse parameter estimation using surface electrical resistivity tomography and borehole data. *Water Resour. Res.* **2014**, *50*, 6828–6849. [[CrossRef](#)]
19. Martorana, R.; Lombardo, L.; Messina, N.; Luzio, D. Integrated geophysical survey for 3D modelling of a coastal aquifer polluted by seawater. *Near Surf. Geophys.* **2014**, *12*, 45–59. [[CrossRef](#)]
20. Pidlisecky, A.; Moran, T.; Hansen, B.; Knight, R. Electrical Resistivity Imaging of Seawater Intrusion into the Monterey Bay Aquifer System. *Groundwater* **2016**, *54*, 255–261. [[CrossRef](#)] [[PubMed](#)]
21. Isaksen, K.; Holmlund, P.; Sollid, J.L.; Harris, C. Three Deep Alpine-Permafrost Boreholes in Svalbard and Scandinavia. *Permafrost. Periglac. Process* **2001**, *12*, 13–25. [[CrossRef](#)]
22. Christiansen, H.H.; Etzelmüller, B.; Isaksen, K.; Juliussen, H.; Farbrot, H.; Humlum, O.; Johansson, M.; Ingeman-Nielsen, T.; Kristensen, L.; Hjort, J.; et al. The thermal state of permafrost in the Nordic Area during the International Polar Year 2007–2009. *Permafrost. Periglac. Process* **2010**, *21*, 156–181. [[CrossRef](#)]
23. Liestøl, O. Pingos, springs, and permafrost in Spitsbergen. *Nor. Polarinst. Årb.* **1975**, 7–29.
24. Haldorsen, S.; Heim, M.; Dale, B.; Landvik, J.Y.; van der Ploeg, M.; Leijnse, A.; Salvigsen, O.; Hagen, J.O.; Banks, D. Sensitivity to long-term climate change of subpermafrost groundwater systems in Svalbard. *Quat. Res.* **2010**, *73*, 393–402. [[CrossRef](#)]
25. Ploeg, M.J.; van der Haldorsen, S.; Leijnse, A.; Heom, M. Subpermafrost groundwater systems: Dealing with virtual reality while having virtually no data. *J. Hydrol.* **2012**, *475*, 42–52. [[CrossRef](#)]
26. Kasprzak, M.; Strzelecki, M.C.; Traczyk, A.; Kondracka, M.; Lim, M.; Migala, K. On the potential for a bottom active layer below coastal permafrost: The impact of seawater on permafrost degradation imaged by electrical resistivity tomography (Hornsund, SW Spitsbergen). *Geomorphology* **2017**, *293*, 347–359. [[CrossRef](#)]
27. Strzelecki, M.C.; Kasprzak, M.; Lim, M.; Świrad, Z.M.; Jaskólski, M.; Pawłowski, Ł.; Modzel, P. Cryo-conditioned rocky coast systems: A case study from Wilczekodden, Svalbard. *STOTEN* **2017**, *607–608*, 443–453. [[CrossRef](#)] [[PubMed](#)]
28. Kasprzak, M.; Łopuch, M.; Głowacki, T.; Milczarek, W. Evolution of Near-Shore Outwash Fans and Permafrost Spreading Under Their Surface: A Case Study from Svalbard. *Remote Sens.* **2020**, *12*, 482. [[CrossRef](#)]
29. Keating, K.; Binley, A.; Bense, V.; Van Dam, R.; Christiansen, H.H. Combined geophysical measurements provide evidence for unfrozen water in permafrost in the Adventdalen Valley in Svalbard. *Geophys. Res. Lett.* **2018**, *45*, 7606–7614. [[CrossRef](#)]
30. Glazer, M.; Dobiński, W.; Marciniak, A.; Majdański, M.; Błaszczak, M. Spatial distribution and controls of permafrost development in non-glacial Arctic catchment over the Holocene, Fuglebekken, SW Spitsbergen. *Geomorphology* **2020**, *358*, 107128. [[CrossRef](#)]
31. Ingeman-Nielsen, T.; Tomaškovičová, S. Multidisciplinary site investigations for improved infrastructure design in Qaanaaq, North Greenland. In Proceedings of the 5th European Conference on Permafrost, Chamonix, France, 23 June–1 July 2018; pp. 156–157.
32. Oldenborger, G.A.; LeBlanc, A.-M. Geophysical characterization of permafrost terrain at Iqaluit International Airport, Nunavut. *J. Appl. Geophys.* **2015**, *123*, 36–49. [[CrossRef](#)]
33. Osterkamp, T.E. Sub-sea permafrost. In *Encyclopedia of Ocean Sciences*; Cochran, J.K., Bokuniewicz, H.J., Yager, P.L., Eds.; Academic Press: Cambridge, MA, USA, 2001; pp. 2902–2912.

34. Rachold, V.; Bolshiyarov, D.Y.; Grigoriev, M.N.; Hubberten, H.-W.; Junker, R.; Kunitsky, V.V.; Overduin, P.; Schneider, W. Nearshore Arctic Subsea Permafrost in Transition. *EOS Trans. Am. Geophys. Union* **2007**, *88*, 149–156. [[CrossRef](#)]
35. Overduin, P.P.; Wetterich, S.; Günther, F.; Grigoriev, M.N.; Grosse, G.; Schirmmester, L.; Hubberten, H.-W.; Makarov, A.S. Coastal dynamics and submarine permafrost in shallow water of the central Laptev Sea, East Siberia. *Cryosphere* **2016**, *10*, 1449–1462. [[CrossRef](#)]
36. Müller, F. On the thermal regime of a high Arctic valley glacier. *J. Glaciol.* **1976**, *16*, 119–133. [[CrossRef](#)]
37. Dobiński, W. Permafrost active layer. *Earth-Sci. Rev.* **2020**, *208*, 103301. [[CrossRef](#)]
38. Czerny, J.; Kieres, A.; Manecki, M.; Rajchel, J. *Geological Map of the SW Part of Wedel Jarlsberg Land, Spitsbergen 1:25,000 (with Explanations)*; Manecki, A., Ed.; Institute of Geology and Mineral Deposits, University of Mining and Metallurgy: Cracow, Poland, 1993; pp. 1–61.
39. Kasprzak, M.; Szymanowski, M. Terrain determinants of permafrost active layer thermal conditions: A case study from Arctic deglaciated catchment (Bratteggdalen, SW Spitsbergen). *PeerJ Prepr.* **2018**, *6*, e27119v2. [[CrossRef](#)]
40. MacKay, D.K. Electrical resistivity measurements in frozen ground, Mackenzie Delta area, Northwest Territories. In *Association Internationale d'Hydrologie Scientifique, Actes du Colloque de Bearest, Reprint Ser*; Inland Waters Branch, Department of Energy, Mines and Resources: Ceuterick, Belgium, 1969; Volume 82, pp. 363–375.
41. King, L.; Seppälä, M. Permafrost thickness and distribution in Finnish Lapland—Results of geoelectrical soundings. *Polarforschung* **1987**, *57*, 127–147.
42. Hauck, C. Frozen ground monitoring using DC resistivity tomography. *Geophys. Res. Lett.* **2002**, *29*, 12-1–12-4. [[CrossRef](#)]
43. Ishikawa, M. Application of DC resistivity imaging to frozen ground investigations. *J. Jpn. Soc. Snow Ice* **2004**, *66*, 177–186. [[CrossRef](#)]
44. Kneisel, C.; Hauck, C. Electrical methods. In *Applied Geophysics in Periglacial Environments*; Hauck, C., Kneisel, C., Eds.; Cambridge University Press: Cambridge, UK, 2008; pp. 3–27.
45. Hilbich, C.; Marescot, L.; Hauck, C.; Loke, M.H.; Mäusbacher, R. Applicability of electrical resistivity tomography monitoring to coarse blocky and ice-rich permafrost landforms. *Permaf. Periglac. Process* **2009**, *20*, 269–284. [[CrossRef](#)]
46. Lewkowicz, A.G.; Etzelmüller, B.; Smith, S.L. Characteristics of discontinuous permafrost based on ground temperature measurements and electrical resistivity tomography, Southern Yukon, Canada. *Permaf. Periglac. Process* **2011**, *22*, 320–342. [[CrossRef](#)]
47. You, Y.; Yu, Q.; Pan, X.; Wang, X.; Guo, L. Application of electrical resistivity tomography in investigating depth of permafrost base and permafrost structure in Tibetan Plateau. *Cold Reg. Sci. Technol.* **2013**, *87*, 19–26. [[CrossRef](#)]
48. Loke, M.H. Electrical Imaging Surveys for Environmental and Engineering Studies. 2000. Available online: <https://pages.mtu.edu/~ctyoung/LOKENOTE.PDF> (accessed on 11 February 2020).
49. Milsom, J. Resistivity methods. In *Field Geophysics*, 3rd ed.; Wiley: Chichester, UK, 2003; pp. 97–116.
50. Reynolds, J.M. Electrical resistivity methods. In *An Introduction to Applied and Environmental Geophysics*, 2nd ed.; Wiley: Chichester, UK, 2011; pp. 289–372.
51. Loke, M.H. *Manual for RES3DINV. Rapid 3-D Resistivity & IP Inversion Using the Least-Squares Method (for 3-D Surveys Using the Pole–Pole, Pole–Dipole, Dipole–Dipole, Rectangular, Wenner, Wenner-Schlumberger and Non-Conventional Arrays). On Land, Aquatic and Cross-Borehole Surveys, Geoelectrical Imaging 2-D & 3-D*; Geotomo Software SDN BHD: Penang, Malaysia, 2013.
52. Doolittle, J.A.; Brevik, E.C. The use of electromagnetic induction techniques in soils studies. *Geoderma* **2014**, *223–225*, 33–45. [[CrossRef](#)]
53. Balkov, E.V.; Fadeev, D.I.; Karin, Y.G.; Manshtein, A.K.; Manshtein, Y.A.; Panin, G.L. A new approach to shallow-depth electromagnetic sounding. *Russ. Geol. Geophys.* **2017**, *58*, 635–641. [[CrossRef](#)]
54. Dafflon, B.; Hubbard, S.S.; Ulrich, C.; Peterson, J.E. Electrical Conductivity Imaging of Active Layer and Permafrost in an Arctic Ecosystem, through Advanced Inversion of Electromagnetic Induction Data. *Vadose Zone J.* **2013**, *12*, 1–19. [[CrossRef](#)]
55. Hayley, K.; Bentley, L.R.; Gharibi, M.; Nightingale, M. Low temperature dependence of electrical resistivity: Implications for near surface geophysical monitoring. *Geophys. Res. Lett.* **2007**, *34*, L18402. [[CrossRef](#)]

56. Telford, W.M.; Geldart, L.P.; Sheriff, R.E. *Applied Geophysics*, 2nd ed.; Cambridge University Press: Cambridge, UK, 1990.
57. Kearey, P.; Brooks, M.; Hill, I. Electrical surveying. In *An Introduction to Geophysical Exploration*, 3rd ed.; Blackwell Science: Hoboken, NJ, USA, 2002; pp. 183–207.
58. Ruppel, C.D.; Herman, B.M.; Brothers, L.L.; Hart, P. ESubsea ice-bearing permafrost on the U.S. Beaufort Margin: 2. Borehole constraints. *Geochem. Geophys. Geosyst.* **2016**, *17*, 4333–4353. [[CrossRef](#)]
59. Sherman, D.; Constable, S. Permafrost extent on the Alaskan Beaufort shelf from surface-towed controlled-source electromagnetic surveys. *J. Geophys. Res. Solid Earth* **2018**, *123*, 7253–7265. [[CrossRef](#)]
60. Gregersen, O.; Eidsmoen, T. Permafrost conditions in the shore area at Svalbard. In Proceedings of the Permafrost Fifth International Conference, Trondheim, Norway, 2–5 August 1988; Senneset, K., Ed.; Tapir Publishers: Trondheim, Norway, 1988; Volume 2, pp. 933–936.
61. Gregersen, O.; Phukan, A.; Johansen, T. Engineering properties and foundation design alternatives in marine Svea clay, Svalbard. In Proceedings of the International Conference on Permafrost 4, Fairbanks, AK, USA, 17–22 July 1983; National Academy of Sciences: Washington, DC, USA, 1983; pp. 384–388.
62. Tsytoich, N.A.; Kronik, Y.A.; Markin, K.F.; Aksenov, V.I.; Samuel'son, M.V. Physical and mechanical properties of saline soils. In Proceedings of the Permafrost Second International Conference, Yakutsk, Russia, 13–28 July 1973; Sanger, F.J., Hyde, P.J., Eds.; National Academy of Sciences: Washington, DC, USA, 1978; pp. 238–247.
63. Zajączkowski, M.; Szczuciński, W.; Plessen, B.; Jernas, P. Benthic foraminifera in Hornsund, Svalbard: Implications for paleoenvironmental reconstructions. *Pol. Polar Res.* **2010**, *31*, 349–375. [[CrossRef](#)]
64. Promińska, A.; Falck, E.; Walczowski, W. Interannual variability in hydrography and water mass distribution in Hornsund, an Arctic fjord in Svalbard. *Polar Res.* **2018**, *37*, 1495546. [[CrossRef](#)]
65. Lech, J.; Walczowski, W. *Data Report on Hydrological Measurements: Norwegian Sea, Fjords, Polar Front, 13.06–09.08.1994, Cruise AREX-94*; Institute of Oceanology PAS: Sopot, Poland, 1994. (In Polish)
66. Włodarska-Kowalczyk, M.; Węśławski, J.M.; Kotwicki, L. Spitsbergen glacial bays macrobenthos—A comparative study. *Polar Biol.* **1998**, *20*, 66–73. [[CrossRef](#)]
67. Olichwer, T.; Tarka, T.; Modelska, M. Chemical composition of groundwaters in the Hornsund region, southern Spitsbergen. *Hydrol. Res.* **2013**, *44*, 117–130. [[CrossRef](#)]
68. Stachnik, Ł.; Majchrowska, E.; Yde, J.C.; Nawrot, A.; Cichała-Kamrowska, K.; Ignatiuk, D.; Piechota, A. Chemical denudation and the role of sulfide oxidation at Werenskioldbreen, Svalbard. *J. Hydrol.* **2016**, *538*, 177–193. [[CrossRef](#)]
69. Oberman, N.G.; Kakunov, B.B. Determination of the thickness of permafrost on the Arctic coast. In Proceedings of the Permafrost Second International Conference, Yakutsk, Russia, 13–28 July 1973; Sanger, F.J., Hyde, P.J., Eds.; National Academy of Sciences: Washington, DC, USA, 1978; pp. 143–147.
70. Osterkamp, T.E.; Baker, G.C.; Harrison, W.D.; Matava, T. Characteristics of the Active Layer and Shallow Subsea Permafrost. *J. Geophys. Res.* **1989**, *94*, 16227–16236. [[CrossRef](#)]

